SUPPLEMENTARY INFORMATION FOR:

Poly(quinone-amine)/nanocarbon composite electrodes with enhanced proton storage capacity

Adriana M. Navarro-Suárez,[a,†] Javier Carretero-González,[b] Teófilo Rojo,[a,c] and Michel Armand[a,*]

[a.] CIC energiGUNE, Albert Einstein 48, 01510 Miñano, Alava, Spain.

[b.] Institute of Polymer Science and Technology, ICTP-CSIC, Juan de la Cierva 3, 28006, Madrid, Spain.

[c.] Inorganic Chemistry Department, P.O. Box 644, University of the Basque Country, 48080 Bilbao, Spain.

[†] Current address: Department of Physics, Chalmers Univ. of Technol., 41296 Gothenburg, Sweden

[*] marmand@cicenergigune.com

Contents:

Supplementary Methods

PREPARATION OF THE BENZOQUINONE-PEO/PPO-DIAMINE TERPOLYMERS ELECTRODES. The different solvents tested were the following: deionized water, perchloric acid (Sigma Aldrich, 70 %), N-methyl-2-pyrrolidone (Sigma Aldrich, 99.5 %), dichloromethane (Sigma Aldrich, > 99.8 %), tetrahydrofuran (Acros, 99.9 %), chloromethane (Sigma Aldrich, > 99.5 %), 1,4-dioxane (Sigma Aldrich, 99.8 %), dimethyl sulfoxide (Sigma Aldrich, 99,9 %), acetonitrile (Sigma Aldrich, 99.8 %), ethyl acetate (Panreac, 100 %), diethyl ether (Sigma Aldrich, 100 %), isopropyl alcohol (Sigma Aldrich, 99.8 %).

CHARACTERIZATION OF THE REDOX POLYMER ELECTRODE MATERIALS. X-Ray diffraction was performed using a D8 X-ray diffractometer (Bruker). Intensity data were collected with CuKα radiation over a 2θ range from 10° to 40° at a step width of 0.03° while the time per step was of 2.7 s.

Changes in the functional groups of the materials developed in this work were followed with Fourier transform infrared spectroscopy. This analysis was performed in a Hyperion 1000 FT-IR spectrometer.

Raman spectra were recorded with a Renishaw spectrometer (Nanonics multiview 2000) operating with an excitation wavelength of 532 nm. The spectrum was acquired after 10 seconds of exposition time of the laser beam to the sample.

The carbonization process of the bi- and ter-polymers were studied by thermogravimetric analysis in a NETZSCH STA 449F3 Jupiter thermal analyzer under an argon stream (Praxair, purity 99.9 %) at a heating rate of 10 °C.min^{-1} up to 900 °C.

Poly[benzoquinone-co-hexamethylenediamine] and poly[benzoquinone-co-(p-phenylenediamine)].

The changes caused in the material by in situ polymerization with MWCNT were followed by XRD and TGA as can be seen in Figure S4. The XRD pattern of the MWCNTs (Figure S4I) showed an intense peak at 2θ = 25.8 ° corresponding to the (002) diffraction. Compared to the normal graphite, 2θ = 26.5 °, this peak showed a downward shift; which was attributed to an increase in the number of sp^2 bonds, C=C layers spacing.[2] The BQhMdA without conductive filler (Figure S4a.I) presented a broad peak, indicating an amorphous structure.[3] When the polymerization occurred around the MWNCTs, the peak at 25.8 ° was broaden but still an intense peak was observed. This pattern indicates a microcrystallinity, meaning that the polymer had regions of aligned chains in small crystallites that diffract and that the remaining chains had no order and contributed to an incoherent scatter.[4] The XRD of the BQpPhdA is shown in Figure S4b.I and shows that the bipolymer still contained crystalline domains due to the π – π stacking between the chains after in situ polymerization.[3]

In order to know the real content (compared to the nominal content) of BQhMdA in the composite, a TGA was performed in air. Figure S4a.II shows the TGA of the MWCNTs, BQhMdA and their composite. The MWCNTs had an initial weight loss temperature at 542 °C and an oxidation temperature at 621 °C. At 900 °C a residual mass of 12 % was found, product of the metal catalyst used to manufacture the nanotubes.[5] The BQhMdA underwent thermal degradation beginning at 250 °C and with a total mass loss of 97 %. The BQhMdA-CNT underwent thermal degradation beginning at 250 °C with a mass loss of 30 %. At 900 °C, the residual mass is 15 %.

Figure S4b.II shows the TGA of the MWCNTs, BQpPhdA and their composite. The MWCNTs started losing mass at a temperature of 542 °C and had an oxidation temperature in air at 621 °C. The BQpPhdA lost 10 % of its mass below 200 °C, due to loss of moisture. Then, the bipolymer underwent a thermal degradation at 310 °C with a total mass loss of 93 %. The absorbance of water seemed less drastic in the BQpPhdA-CNT as only ≈ 1 % of mass was loss below 200 °C. The thermal degradation of the composite started at 310 °C with a mass loss of 32 %. At 900 °C, the residual mass was 15 %.

We have also studied in detail the distribution of the polymer and the MWCNTs in the composite electrode by using Transmission Electron Microscopy (TEM). Figure S5 shows a bulk fraction of the BQpPhdA polymer highly filled with the conductive fillers (*i.e.* MWCNT) (Figure S5a). Moreover, there it was also evidenced by TEM a fraction of the polymer located on the surface of the MWCNT for the composites prepared *in situ* with MWCNT in EtOH. BQpPhdA-MWCNT, achieved 472 mAh.g^{-1} at 80 mA.g^{-1} confirming the impact of the presence of an intimate interface between the polymer and the nanocarbon on the electrochemical properties.

Herein, Raman, XRD and FTIR (Figure S6) were also used to follow the different structural and compositional variations of the polymer-based electrodes occurring during the galvanostatic cycling. To decrease the signal coming from the MWCNTs in the previous techniques, the weight ratio bipolymer:MWCNT was modified to 95:5.

By decreasing the amount of MWCNTs in the composite, we observed a clear loss of crystallinity in the BQhMdA-MWCNT electrode material (Figure S6a.I). After charge and discharge, the more organized regions were not observed anymore. In the case of the BQpPhdA-MWCNT (Figure S6b.I)), the aromatic composite presented a semi-crystalline structure, caused by the presence of MWCNTs. After charge and discharge, the broad features of the amorphous regions overshadowed the crystalline peaks and still some microcrystallinity was observed.

Figure S6a.II shows the Raman spectra of BQhMdA-MWCNT before cycling and after charge and discharge. The only appreciable peaks are at ≈ 1601 cm^{-1} and ≈ 1337 cm^{-1} and likely correspond to the G and D band of the MWCNTs, respectively. The G peak corresponds to the E_{2g} phonon at the Brillouin zone center. The D peak is due to the breathing modes of sp^2 rings and requires a defect for its activation.[6] These defects that activate the D band may be caused by the presence of the polymer fraction at the surface of the MWCNT. These bands were not affected during the oxidation and reduction of the polymer, meaning no more defects were included in the material with cycling. However, these peaks were also overlapping with the typical Raman shifts from the hydroquinone molecules. In this case, the peaks at ~1601 cm^{-1} and ~1337 cm^{-1}, would correspond to the C=C and C-C vibrations, respectively.[7] These vibrations did not change with cycling; therefore, the bands did not change neither.

The Raman spectra of BQpPhdA-MWCNT (Figure S6b.II)) showed several peaks that corresponded to the p-phenylene-diamine structure. Badawi *et al.*[8] have reported a possible assignation of these peaks: 1598 cm^{-1} (ring deformation), 1489 cm^{-1} (ring stretch deformation), 1470 cm^{-1} (ring stretch deformation and p-CH in plane bending), 1320 cm^{-1} (ring-N stretch and ring breathing), and 1168 cm^{-1} (p-CH in plane bending). As the redox processes of the BQpPhdA involved the active moieties of the p-phenylenediamine, changes in the spectra were expected; however, the reaction was difficult to follow by Raman because of the close vicinity of all the bands.

Poly[benzoquinone-co-hexamethylenediamine-co-PEO/PPO] and poly[benzoquinone-co-(p-phenylenediamine)-co-PEO/PPO].

In order to develop processable electrodes, benzoquinone and hexamethylenediamine were copolymerized with PEO/PPO derivatives. The polymers formed are depicted in Figure S7. Table S3 relates the PEO/PPO linkers with the terpolymers shown in Figure S7 as well as their theoretical capacity.

To develop processable electrodes, these materials should be soluble in a solvent with low evaporation temperature so it can be easily eliminated after casting/processing. In addition, the terpolymers must not be soluble in the electrolyte in which they were going to be electrochemically tested (*i.e.* this work: 0.1 M perchloric acid in water), the results of these tests are summarized in Table S4. Most of the terpolymers were insoluble or partially soluble in the solvents tested. Only two terpolymers were soluble in NMP while still being insoluble in 0.1 M perchloric acid in water: BQhMdA400 and BQpPhdA900.

Figure S8 shows the effect of the sodium chloride on the BQpPhdA900 electrode before and after washing off the NaCl with water. By washing with water the NaCl introduced during the polycondensation process, the increment on the surface would enhance the pseudo-capacitive reactions, enlarging the final total capacity.

Table S1. Reaction conditions of the bipolymer formation.

Entry	$H_2N-R^1-NH_2$	Product (Copolymer)	Time (h)
1		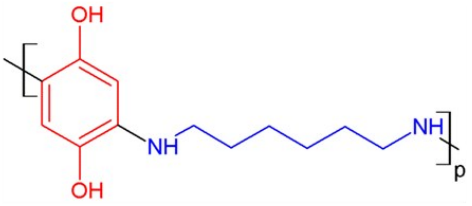	14
2	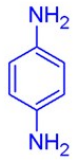	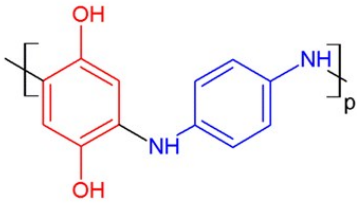	14

Table S2. List of PEO/PPO molecules used as linkers in the preparation of the terpolymers.

$H_2N-R_2-NH_2$	Acronym
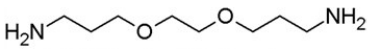 1,10-Diamino-4,7-dioxadecane	Dioxa
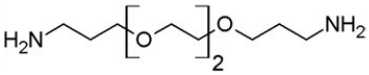 4,7,10-Trioxa-1,13-tridecanediamine	Trioxa
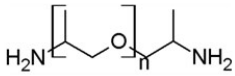 Poly(propylene glycol) bis(2-aminopropyl ether) n ≈ 6.1	D-400
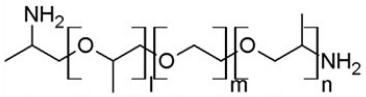 O,O′-Bis(2-aminopropyl) polypropylene glycol-block-polyethylene glycol-block-polypropylene glycol 500 m ≈ 9 l + n ≈ 3.6	ED-600
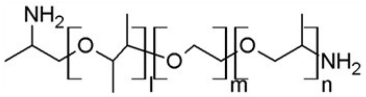 O,O′-Bis(2-aminopropyl) polypropylene glycol-block-polyethylene glycol-block-polypropylene glycol 800 m ≈ 12.5 l + n ≈ 6	ED-900

Table S3. Poly[benzoquinone-co-hexamethylenediamine-co-PEO/PPO] and Poly[benzoquinone-co-(p-phenylenediamine)-co-PEO/PPO] theoretical capacities related to the PEO/PPO linker.

Entry	Remarks	PEO/PPO Acronym	Terpolymer Theoretical Capacity $mAh.g^{-1}$
3a	--	Dioxa	211
3b	--	Trioxa	194
3c	PPO $n \approx 6.1$	D-400	146
3d	$m \approx 9$; $(l+n) \approx 3.6$	ED-600	115
3e	$m \approx 12.5$; $(l+n) \approx 6$	ED-900	87
4a	--	Dioxa	321
4b	--	Trioxa	295
4c	$n \approx 6.1$	D-400	222
4d	$m \approx 9$; $(l+n) \approx 3.6$	ED-600	174
4e	$m \approx 12.5$; $(l+n) \approx 6$	ED-900	131

Table S4. Solubility tests results of the Poly[benzoquinone-co-hexamethylenediamine-co-PEO/PPO]and Poly[benzoquinone-co-(p-phenylenediamine)-co-PEO/PPO].

Solvent	**3a**	**3b**	**3c**	**3d**	**3e**	**4a**	**4b**	**4c**	**4d**	**4e**
Water	No	No	No	No	No	No	No	No	No	No
$HClO_4$	No	No	No	No	No	No	No	No	No	No
NMP	Partially	Partially	**Yes**	No	No	Partially	Partially	Partially	No	**Yes**
CH_2Cl_2	Partially	Partially	Partially	No	No	Partially	Partially	Partially	No	Partially
THF	Partially	Partially	Partially	No	No	Partially	Partially	Partially	No	Partially
CH_3Cl	Partially	Partially	Partially	No	No	Partially	Partially	Partially	No	Partially
Dioxane	Partially	Partially	Partially	No	No	Partially	Partially	Partially	No	Partially
DMSO	Partially	Partially	Partially	No	No	Partially	Partially	Partially	No	Partially
ACN	Partially	Partially	Partially	No	No	Partially	Partially	Partially	No	Partially
Ethyl Acetate	Partially	Partially	Partially	No	No	Partially	Partially	Partially	No	Partially
Diethyl Ether	Partially	Partially	Partially	No	No	Partially	Partially	Partially	No	Partially
Isopropanol	Partially	Partially	Partially	No	No	Partially	Partially	Partially	No	Partially

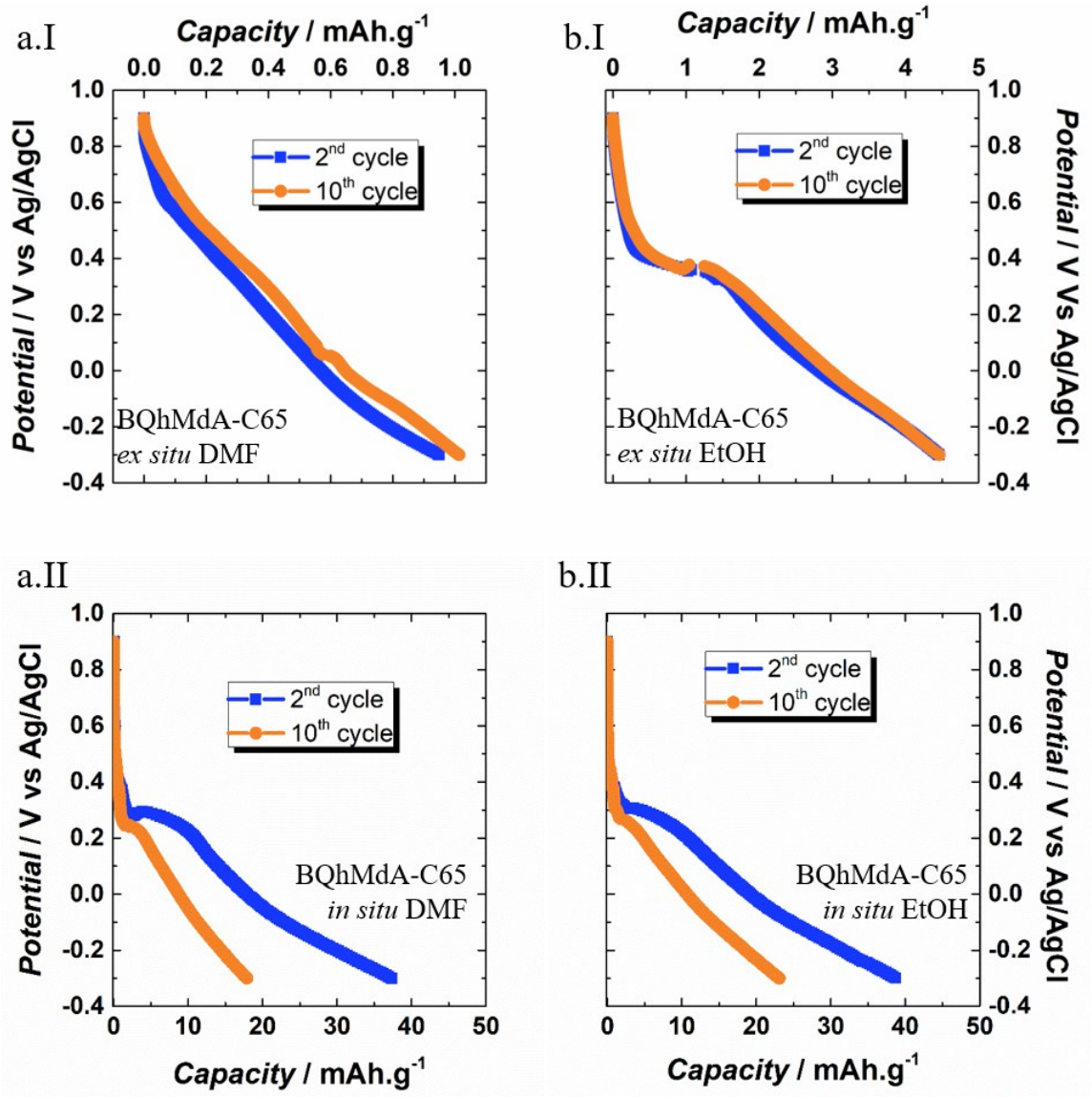

Figure S1. Electrochemical comparison of the BQhMdA synthesized in DMF (a) and in EtOH (b). Inclusion of the C65 carbon particles after polymerization (I) and during polymerization (II).

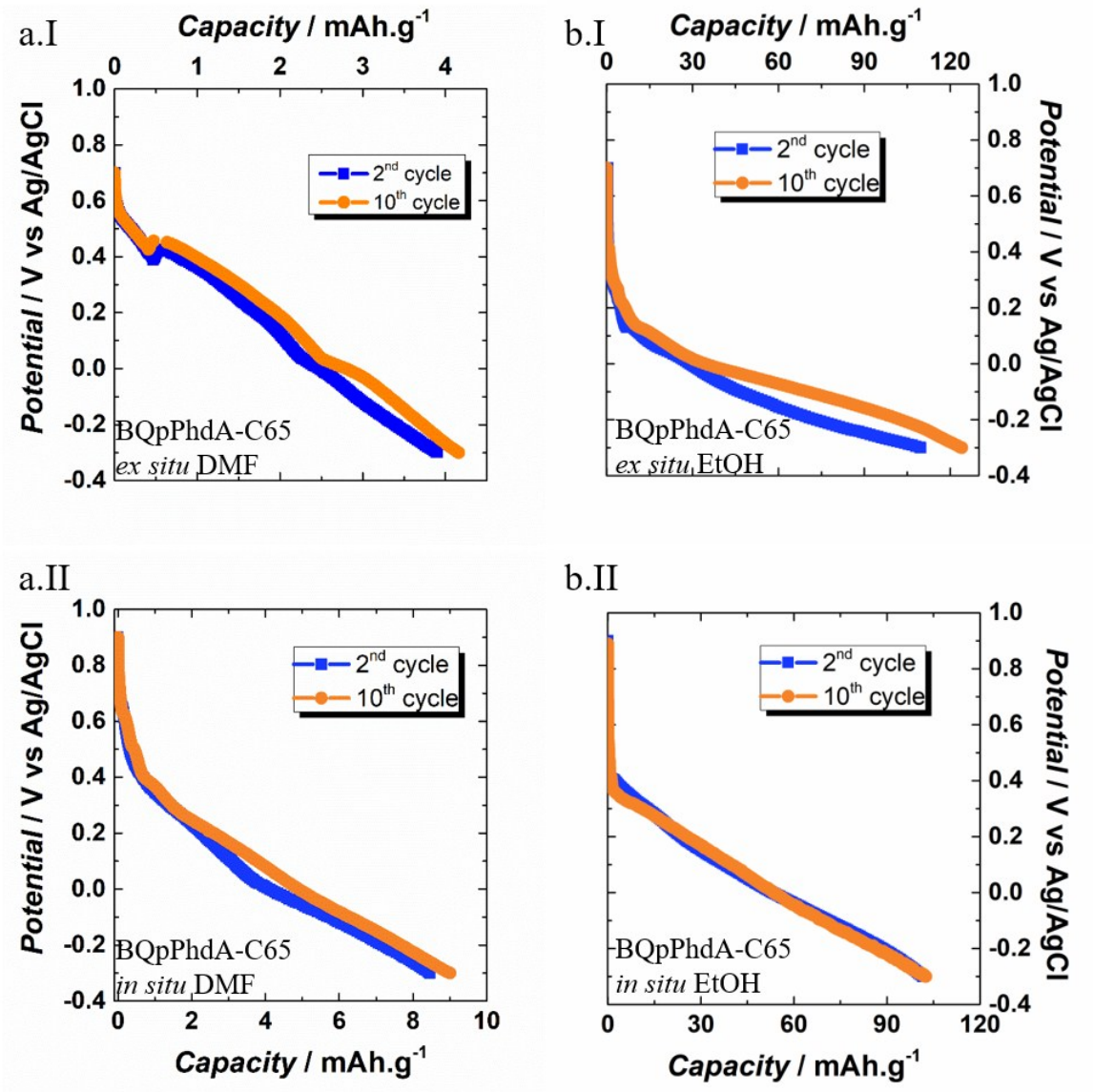

Figure S2. Electrochemical comparison of the BQpPhdA synthesized in DMF (a) and in EtOH (b). Inclusion of the C65 carbon particles after polymerization (I) and during polymerization (II).

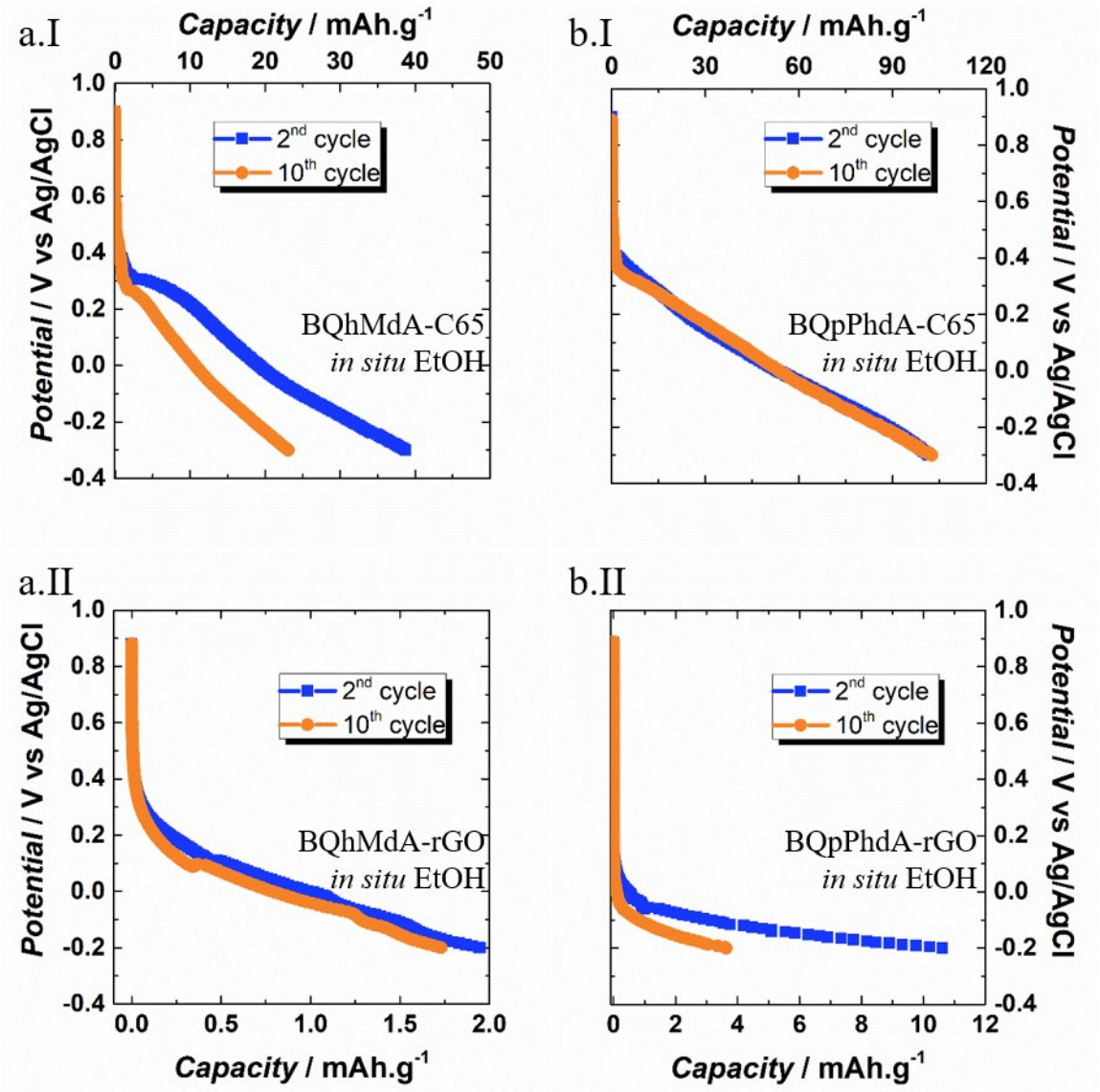

Figure S3. Electrochemical comparison of the BQhMdA (a) and the BQpPhdA (b) synthesized *in situ* with C65 (I) and rGO (II).

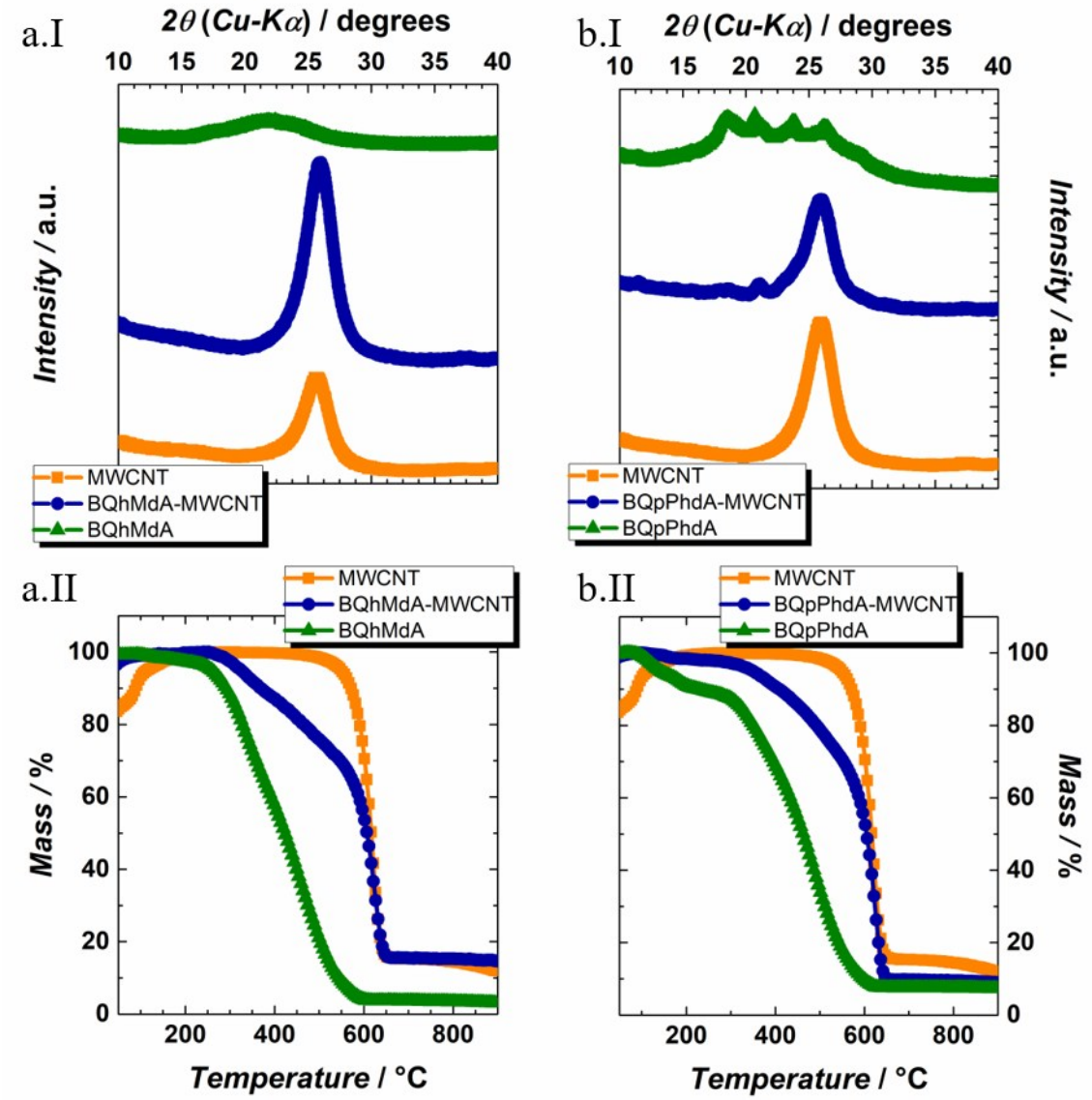

Figure S4. XRD (I) and TGA (II) of the BQhMdA (a), BQpPhdA (b), MWCNT and their composites.

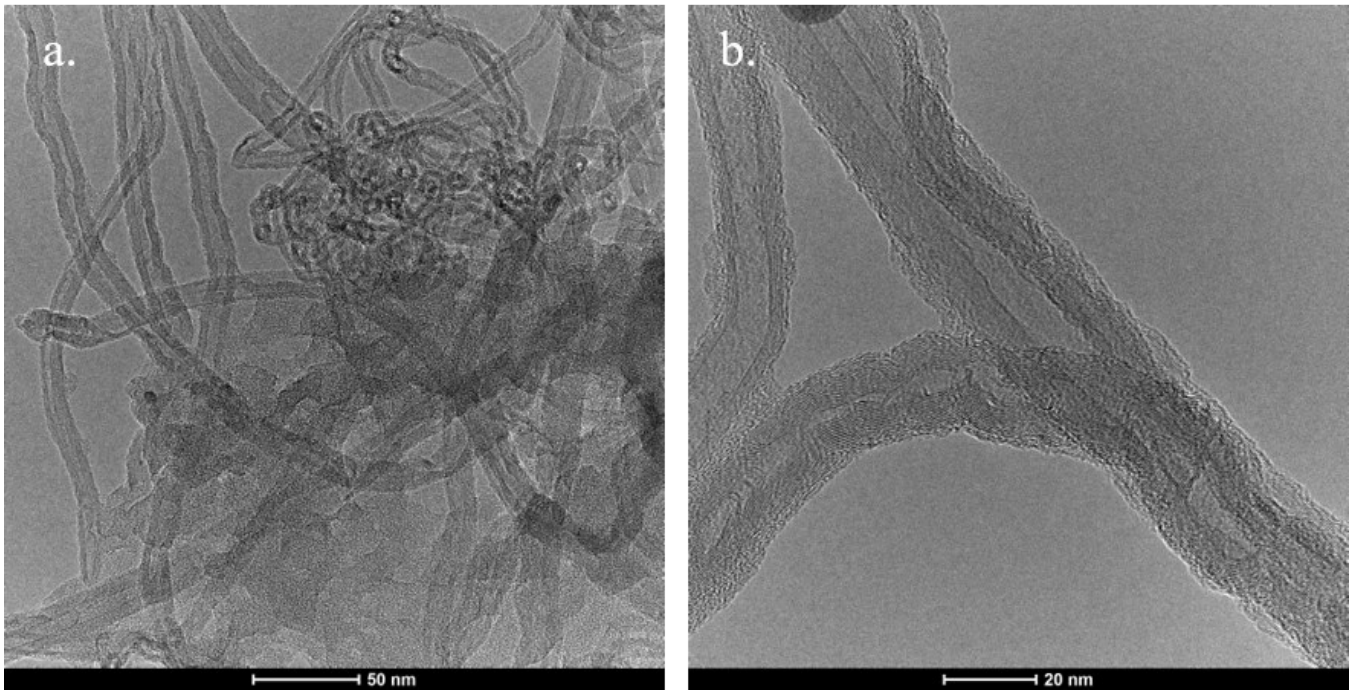

Figure S5. TEM images of BQpPhdA-MWCNT synthesized in EtOH showing the bulk structure (a) and the MWCNT's surface (b).

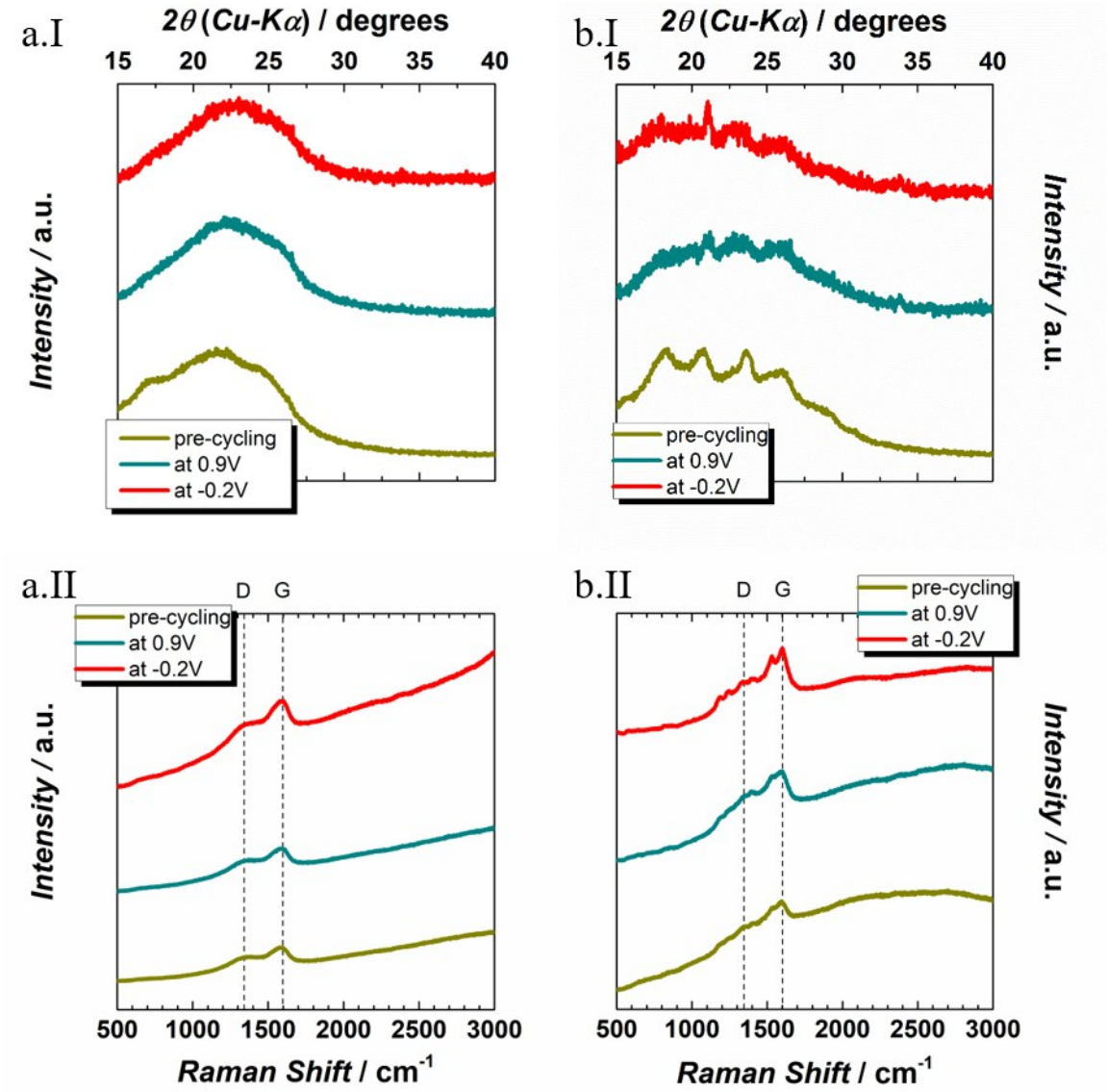

Figure S6. XRD (I) and Raman (II) plots of the BQhMdA-MWCNT (a) and BQpPhdA-MWCNT (b) before cycling, and after charge and discharge.

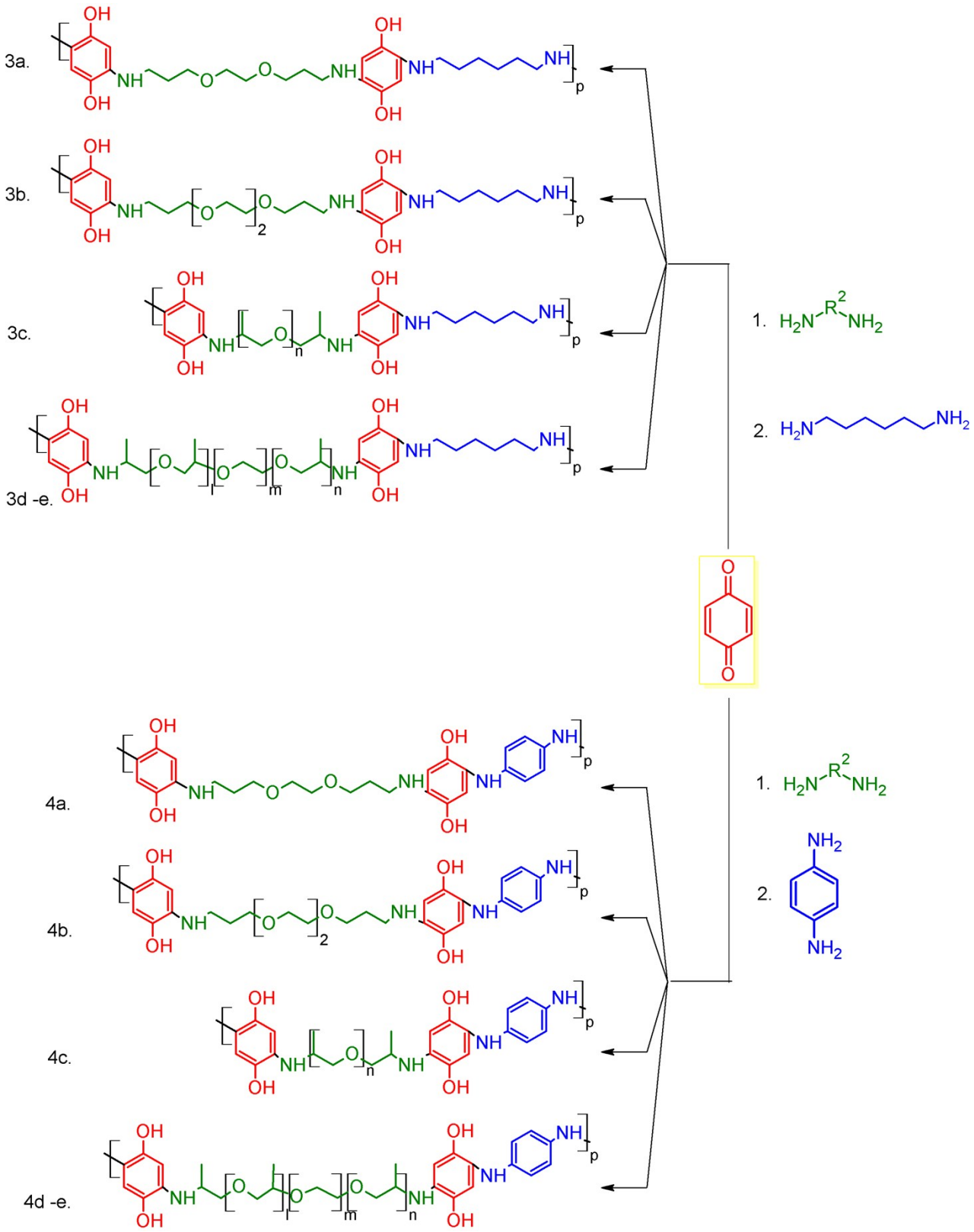

Figure S7. Polymerization of Poly[benzoquinone-co-hexamethylenediamine-co-PEO/PPO] and Poly[benzoquinone-co-(p-phenylenediamine)-co-PEO/PPO].

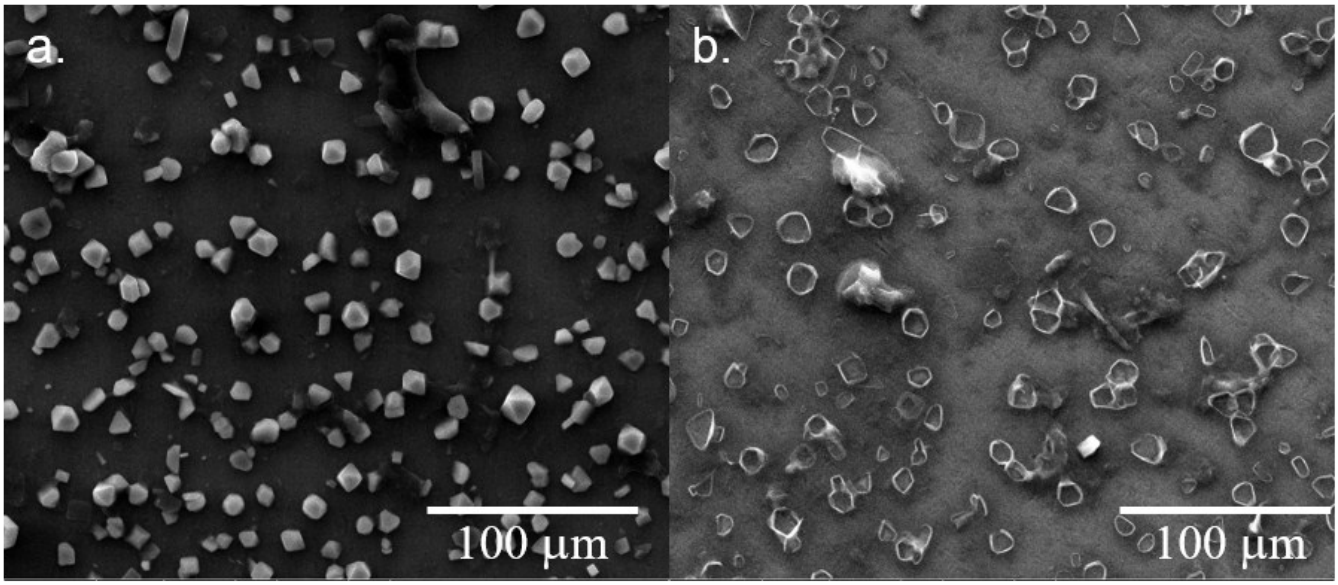

Figure S8. SEM images of the BQpPhdA900 *in situ* with MWCNT electrode before (a) and after (b) washing off the NaCl with water.

REFERENCES

(1) Wang, M.; Duan, X.; Xu, Y.; Duan, X. *ACS Nano* **2016**, *10* (8), 7231–7247.

(2) Zhang, H.-B.; Lin, G.-D.; Zhou, Z.-H.; Dong, X.; Chen, T. *Carbon N. Y.* **2002**, *40* (13), 2429–2436.

(3) Klug, H. P. (Harold P.; Alexander, L. E. (Leroy E. *X-ray diffraction procedures for polycrystalline and amorphous materials*, 2nd ed.; John Wiley & Sons, 1974.

(4) Lee, T. H.; Boey, F. Y. C.; Khor, K. A. *Polym. Compos.* **1995**, *16* (6), 481–488.

(5) Lehman, J. H.; Terrones, M.; Mansfield, E.; Hurst, K. E.; Meunier, V. *Carbon N. Y.* **2011**, *49*, 2581–2602.

(6) Casiraghi, C.; Hartschuh, A.; Qian, H.; Pliscanec, S.; Georgia, C.; Fasoli, A.; Novoselov, K. S.; Basko, D. M.; Ferrari, A. C. *Nano Lett.* **2009**, *9* (4), 1433–1441.

(7) Stammreich, H.; Teixeira Sans, T. *J. Chem. Phys.* **1965**, *42* (3), 920–931.

(8) Badawi, H. M.; Förner, W.; Ali, S. A. *Spectrochim. Acta Part A Mol. Biomol. Spectrosc.* **2013**, *112*, 388–396.